# Investigation of Time-Reversal Based Far-Field Wireless Power Transfer From Antenna Array in a Complex Environment

## HONG SOO PARK, (Student Member, IEEE), AND SUN K. HONG, (Member, IEEE)

School of Electronic Engineering, Soongsil University, Seoul 06978, South Korea

Corresponding author: Sun K. Hong (shong215@ssu.ac.kr)

**ABSTRACT** The performance of time-reversal (TR) based far-field wireless power transfer (WPT) from an antenna array in a complex propagation environment is investigated in comparison with conventional array-based beamforming (BF). A two-step experiment is performed, namely 1) the propagation stage and 2) rectification stage. In the propagation stage, signal transmission is measured between the transmit array and receive antenna in an indoor multipath environment, for line-of-sight (LOS) and non-line-of-sight (NLOS) scenarios. The results demonstrate that TR results in higher peak voltage compared to BF given the same average transmit power. In addition, while BF loses its ability to selectively send waves at the receiver due to impairment of the beam from multipath, TR can selectively focus waves at the receiver by inherently taking advantage of multipath. In the rectification stage, the resulting signals from the propagation stage are fed into a broadband rectifier for RF-to-DC conversion. It is shown that the signals received using TR lead to higher rectified DC voltage and rectification efficiency. The overall results suggest that TR can outperform BF with higher rectification efficiency given the same average transmit power. Through optimization of the TR pulse interval, array configuration and transmit power, further improvement in the performance of TR based WPT in a complex propagation environment is possible.

**INDEX TERMS** Time-reversal, complex propagation environment, wireless power transfer, antenna array, beamforming, broadband rectifier, rectification efficiency.

## I. INTRODUCTION

Far-field (radiative) wireless power transfer (WPT) is an emerging technology for wirelessly charging small, low power devices, which can be widely utilized in the fields of mobile devices, internet of things (IoT), sensors, and biomedical devices [1]–[7]. Unlike near-field WPT based on magnetic coupling, far-field WPT is based on sending and receiving radiated electromagnetic waves, which allows for transmission of power at longer range (i.e. beyond few meters). For far-field WPT, array-based beamforming (BF) is commonly used to focus electromagnetic energy at desired locations [8]–[14]. In [8]–[12], a retrodirective BF is proposed, a well-known beamforming technique implemented through phase conjugation using a retrodirective array. In [13], [14], adaptive beamforming with massive multiple-input multiple-output (mMIMO) using a large-scale

The associate editor coordinating the review of this manuscript and approving it for publication was Shah Nawaz Burokur.

antenna array is considered based on the theoretical development for simultaneous wireless information and power transfer applications. However, potential disadvantages of BF arise especially in a complex propagation environment (e.g. indoor environment where multiple scatterers and reflecting walls exist), which could impair the beam generated by the array. In addition, for mMIMO beamforming, the configuration and operation of the system could be quite complicated due to a large number of antennas used. One way to overcome such drawbacks of BF would be to employ time-reversal (TR) based far-field WPT [15]–[20]. TR applied in a complex propagation environment allows for spatial and temporal wave focusing by taking advantage of multipath, thereby selectively concentrating electromagnetic power at a desired location even with a single transmit antenna [20]–[26]. In particular, previous studies have demonstrated that sending TR waveforms can deliver higher peak power (compared to sending narrowband signals) at desired locations in a complex propagation environment [17], [20], [26]. But the antenna
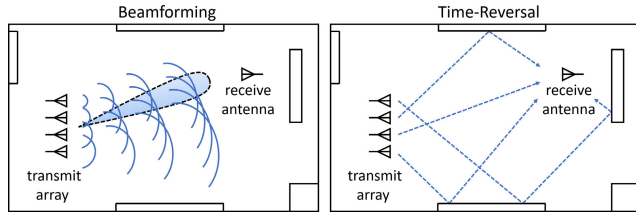
**FIGURE 1.** Illustration of array-based far-field wireless power transfer via beamforming (left) and time-reversal (right) in a complex propagation environment.



**FIGURE 2.** Relation between the relative position of the receive antenna to the transmit array and phase at each transmit element.

configuration used in these studies was limited to a single transmit antenna case. Since many recently proposed far-field WPT systems employ array-based BF, it would be necessary to analyze the performance of TR based far-field WPT from an antenna array in comparison to array-based BF.

The purpose of this paper is to investigate TR based WPT in an indoor environment consisting of an antenna array on the transmit side, so as to directly compare its performance with that of BF using the same array. Successful far-field WPT depends not only on effectively delivering RF power to a receive antenna, but also on efficient rectification of the received RF to DC [27]–[30]. Hence, we present our investigation through a two-step experiment: 1) the wave propagation stage where measurements are performed in an actual indoor environment between the transmit array and receive antenna and 2) the rectification stage where the received signals are fed into a broadband rectifier to measure DC voltage.

This paper is organized as follows. In Section II, the procedures for array-based far-field WPT via BF and TR implemented in our study are described and a theoretical basis for analyzing the performance of TR vs. BF is provided. Section III describes the experiment setup, which is divided into the wave propagation and rectification stages. In Section IV, the simulated and measured results from the wave propagation stage are presented. In Section V, the measured results of the rectification stage are presented. Finally, Section VI concludes the paper with a quick summary and implications of the results.

## II. ARRAY-BASED BEAMFORMING VERSUS TIME-REVERSAL

An array-based far-field WPT scenario in a complex, multi-path environment would consist of a multi-element transmit antenna array and a receiver (or multiple discrete receivers) represented with a single receive antenna. Fig. 1 illustrates the mechanism of BF (left) and TR (right) based wireless power transmission. In both cases, the purpose is to deliver maximum electromagnetic energy at a desired receiver. However, there is a distinct difference in that BF sends electromagnetic waves by phasing the array elements to form a beam in the direction of the receiver, while TR sends a tailored waveform that will allow the transmitted electromagnetic waves to take advantage of multipath. In a practical scenario, the receiver
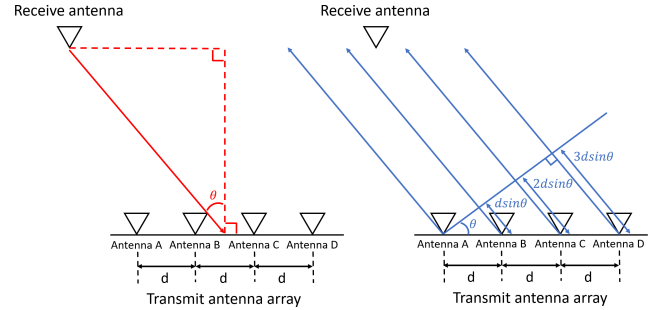
should include a separate transmitter that broadcasts a beacon signal. The beacon signal is broadcast only when the receiver needs wireless power. This beacon signal propagates through the environment and is received by the transmit antenna array (which means that the transmit antenna array also requires a receiver) and processed to generate either the phase necessary for BF or the time-reversed waveforms for TR. The beacon signal can be broadcast periodically to update the information on the propagation environment. The update interval may need to be adjusted depending on the level of mobility and fluctuations in the environment. Note that the presence of the beacon transmitter/receiver in Fig.1 is omitted for simplicity of illustration. In the following subsections, the mechanisms of BF and TR are briefly discussed.

### A. BEAMFORMING WITH ANTENNA ARRAY

BF is a technique based on an antenna array in which the phase and amplitude of each array element is adjusted to generate the main beam in a desired direction. BF in a typical WPT scenario is carried out in a retrodirective fashion. That is, a beacon signal sent from a desired receiver is first collected by the transmit antenna array in the receive mode, allowing the information about the receiver location to be extracted in the form of relative phase differences between the array elements. The transmit signals are then fed with the conjugated phase to direct the beam at the receiver. Considering an $N$-element linear array as used in our experiment, Fig. 2 illustrates the phase required to direct the beam at the corresponding receiver. For a receiver located at an angle $\theta$ from the broadside direction of the transmit antenna array, the relative phasing of each element should correspond to

$$\phi_n = (n-1)\beta d \sin \theta, \quad n = 1, \ldots, N, \quad (1)$$

where $d$ is the array element spacing and $\beta$ is the free space wave number. Here we use an element spacing of $\lambda/2$ to avoid grating lobes and the corresponding phase constant $\beta d$ becomes $\pi$. By applying the phase in (1) to each element, it is possible to form a beam in the direction of $\theta$. However, in a complex propagation environment, the beacon signal will travel through various paths and distort the wavefront, causing inaccurate phase information to be extracted. That is, $\phi_n$ may not accurately represent the values in (1).
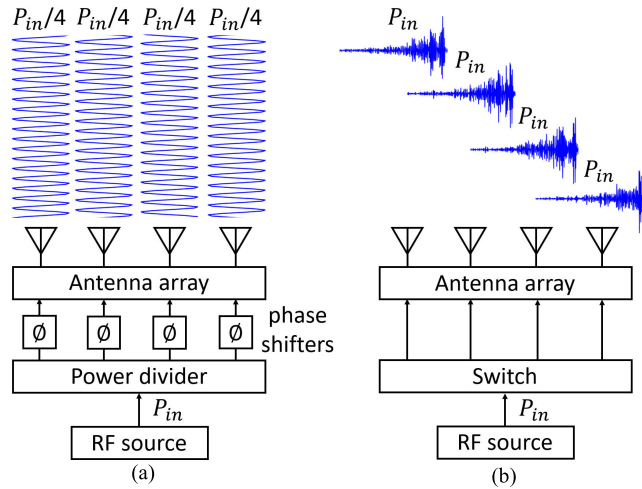
FIGURE 3. A notional transmit system for : (a) BF and (b) TR.



FIGURE 4. An example signal at each step of the TR process: (a) a beacon signal p(t) (a 5 ns Gaussian pulse), (b) the beacon signal received by an array element $b_n(t; T)$ with T= 200ns, (c) the time-reversed signal $x_{n,TR}(t)$ used for power transmission, and (d) the resulting signal at the receiver as a result of wave focusing $y_{n,TR}(t)$.

In an effort to draw a comparative description relative to TR, we describe the process of signal transmission via BF in terms of the time-domain linear system representation. The impulse responses between each transmit element and the receive antenna can be represented as

$$h_n(t) = F^{-1}\left\{S_{r,n}(\omega)\right\}, \tag{2}$$

where $F^{-1}\{\cdot\}$ denotes the inverse Fourier transform and $S_{r,n}(\omega)$ represents the transfer function between each transmit element in the array and the receive antenna. The input signal fed into each transmit element is assumed to be a continuous-wave (CW) waveform that is amplified to a desired level and phase-shifted according to (1), i.e.

$$x_{n,BF}(t) = A\cos(\omega_0 t - \phi_n), \tag{3}$$

where $\omega_0 = 2\pi f$ is the signal frequency and $A$ is a scalar constant representing signal amplification. A notional transmit system for BF is illustrated in Fig. 3a, where CW generated from the source (including amplifier) is divided $N$-way, phase shifted, and radiated simultaneously through the array. The resulting signal at the receive antenna is then expressed as

$$y_{n,BF}(t) = h_n(t) * x_{n,BF}(t), \tag{4}$$

where $*$ denotes convolution. The sum of each output signal $y_{n,BF}(t)$ becomes the resulting signal of BF as follows:

$$y_{BF}(t) = \sum_{n=1}^{N} y_{n,BF}(t), \tag{5}$$

which is then send to the rectifier for conversion to DC power.

### B. TIME REVERSAL WITH ANTENNA ARRAY

In a complex propagation environment, scatterers and reflecting walls cause multipath. A short pulse transmitted in this environment undergoes spreading as it travels through a number of different trajectories, thereby arriving at the receiver 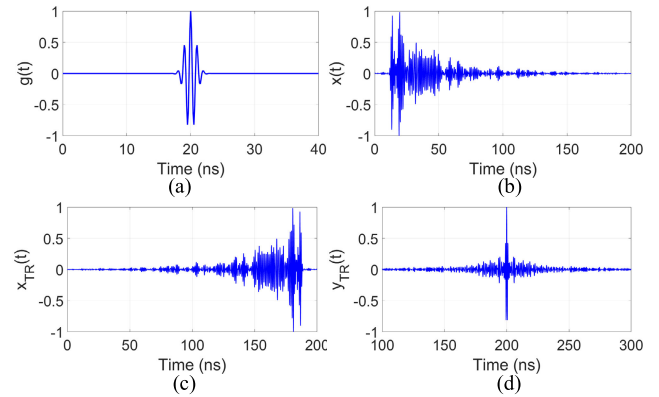at different times. The TR technique, when used with a short pulse, can take advantage of such a multipath environment to enable selective wave focusing at a desired location. Here we describe the process of TR utilized with the same $N$-element linear array used for BF. The way we apply TR here is that the array elements are operated in a switching manner, where only one element transmits at a time unlike BF. It is possible for all array elements to transmit simultaneously for TR. However, this would require each array element to have its own source (arbitrary waveform generator) to generate TR signals. Transmitting in a switched mode allows only one source to be used just like BF as shown in Fig. 3.

For TR based WPT, a beacon signal is also sent from a desired receiver to be collected by the transmit antenna array. The beacon signal in this case is assumed to be a short pulse (containing the bandwidth of interest) represented as $p(t)$. Fig. 4(a) shows an example of $p(t)$, which is used in the experiment (more detail to be discussed in the proceeding sections). The signal received by each array element for a duration of $T$ is expressed as (see Fig. 4(b) for example)

$$b_n(t; T) = p(t) * h_n(t; T) \tag{6}$$

where $h_n(t)$ is the impulse response between the receiver and $n^{th}$ array element. Here, $b_n(t)$ should approximately represent $h_n(t)$ over the bandwidth of $p(t)$. The signal fed into each array element for power transmission is a time-reversed version of $b_n(t)$(see Fig. 4(c)), i.e.

$$x_{n,TR}(t) = Bb_n(nT - t), \tag{7}$$

where $B$ represents signal amplification. Note that each $x_{n,TR}(t)$ is shifted by $nT$, so as to be transmitted from the corresponding array element with an interval of $T$ in a successive manner via switching, as depicted in Fig. 3(b). Since $x_{n,TR}(t)$ contains the inverse profile of the multipath time-delays as a result of time-reversal, the effects of multipath can be "undone" as the signal propagates back to the receiver, allowing the waves to coherently arrive at the receiver at a particular point in time (i.e. $t = nT$). This wave focusing
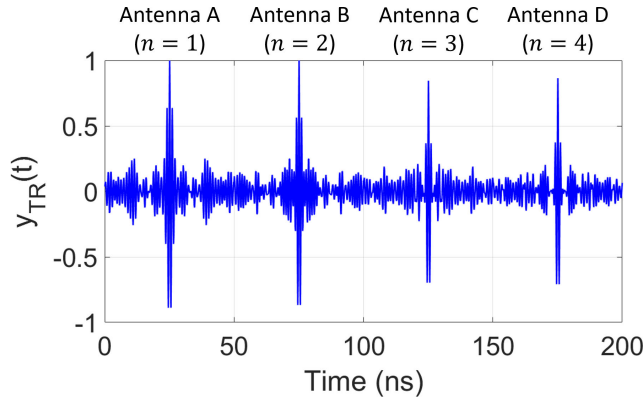
**FIGURE 5.** An example of $y_{TR}(t)$ when N = 4 and T = 50 ns.

allows for the approximate reconstruction of the original short pulse. Accordingly, the resulting signal at the receive antenna is expressed as (see Fig. 4(d))

$$
\begin{aligned}
y_{n,TR}(t) &= x_{n,TR}(t) * h_n(t) \\
&= Bp(nT - t) * [h_n(nT - t) * h_n(t)], \quad (8)
\end{aligned}
$$

indicating that $y_{n,TR}(t)$ approximately represents an autocorrelation of $h_n(t)$. The sum of each $y_{n,TR}(t)$ is

$$
y_{TR}(t) = \sum_{n=1}^{N} y_{n,TR}(t), \quad (9)
$$

which is a train of $N$ short pulses with an interval of $T$ as shown in Fig. 5. This pulse train is repeatedly received and sent to the rectifier for conversion to DC power.

### C. PEAK RECEIVED POWER RATIO BETWEEN BEAMFORMING AND TIME REVERSAL

The power transmission performance between TR vs. BF can be compared by defining a term referred to as the peak received power ratio (PRPR), i.e.

$$
PRPR = \frac{\max\{y_{TR}^2(t)\}}{\max\{y_{BF}^2(t)\}}, \quad (10)
$$

which can be obtained directly from measured signals and used as a performance metric of TR WPT vs. BF WPT.

We can also derive a theoretical expression of *PRPR* from the signal equations in the preceding subsections. For simplicity of derivation, the beacon signal in the TR process $p(t)$ is assumed to be an ideal impulse (i.e. $p(t) = \delta(t)$). The denominator in (10) represents the signal level from BF, which is a narrowband signal (CW). Hence, it can be represented using the frequency domain terms as

$$
\begin{aligned}
\max\{y_{BF}^2(t)\} &= \left| \left\{ \sum_{n=1}^{N} H_n(\omega_0) A e^{-j\phi_n} \right\} \right|^2 \\
&= A^2 \left| \left\{ \sum_{n=1}^{N} |H_n(\omega_0)| e^{j(\alpha_n - \phi_n)} \right\} \right|^2, \quad (11)
\end{aligned}
$$

where $Ae^{-j\phi_n}$ and $H_n(\omega) = |H_n(\omega)| e^{j\alpha_n}$ are the Fourier transform of $x_{n,BF}(t)$ and $h_n(t)$, respectively. The numerator

in (10) represents the maximum peak amplitude among $N$ pulses resulting from TR (Fig. 5), which occurs at $t = nT$ (where $n$ is associated with the pulse having the highest peak). Setting $n = 1$ to simplify derivation, we can express $\max\{y_{TR}^2(t)\}$ using the frequency domain terms and the inverse Fourier relation as (subscript $n$ is removed)

$$
\begin{aligned}
\max\{y_{TR}^2(t)\} &= \left[ \frac{B}{2\pi} \int_{-\infty}^{\infty} H^*(\omega)e^{-j\omega T} H(\omega)e^{j\omega t} d\omega \right]^2_{t=T} \\
&= \frac{B^2}{4\pi^2} \left[ \int_{-\infty}^{\infty} |H(\omega)|^2 d\omega \right]^2, \quad (12)
\end{aligned}
$$

where $e^{-j\omega T}$ is associated with a time shift $T$ in $h(T - t)$.

Here we assume that both TR and BF transmit the same average power $P_{in}$ (as illustrated in Fig. 3), which can then be expressed in terms of the signal amplification factors $A$ and $B$ for $x_{n,BF}(t)$ and $x_{n,TR}(t)$, respectively, as

$$
P_{in} = \frac{NA^2}{2Z_{in}} = \frac{B^2}{Z_{in}T} \int_T |h(T - t)|^2 dt, \quad (13)
$$

where $Z_{in}$ is the input impedance of each array element (real-valued). Solving for $A$ and $B$, we get

$$
A = \sqrt{\frac{2P_{in}Z_{in}}{N}} \quad (14)
$$

and

$$
B = \sqrt{\frac{Z_{in}P_{in}T}{\int_T |h(T - t)|^2 dt}} \approx \sqrt{\frac{Z_{in}P_{in}T}{\frac{1}{2\pi} \int_{-\infty}^{\infty} |H(\omega)|^2 d\omega}}. \quad (15)
$$

In (15), $h(T - t)$ is a time-reversed version of $h(t)$ for a time duration of $T$, which can approximately be expressed with the frequency domain terms by Parseval's relation. Substituting (11) - (15) into (10), *PRPR* can consequently be represented as

$$
PRPR = \frac{NT}{4\pi} \frac{\left[ \int_{-\infty}^{\infty} |H(\omega)|^2 d\omega \right]}{\left| \left\{ \sum_{n=1}^{N} |H_n(\omega_0)| e^{j(\alpha_n - \phi_n)} \right\} \right|^2}, \quad (16)
$$

which implies that *PRPR* can simply be obtained using the transfer function (impulse response) between the transmit and receive antennas, the time duration $T$ of the impulse response used for TR, and the number of transmit array elements. In other words, the level of *PRPR* should depend on the propagation environment and the array setup. This means that in a complex propagation environment, *PRPR* should be large ($\gg 1$) and TR is expected to deliver a peak power higher than BF. On the contrary, in an environment where little or no multipath exists, *PRPR* should be small (near or $<1$), indicating little or no advantage of using TR over BF. A qualitative analysis of *PRPR* in some example environments with different multipath conditions is provided in the Appendix.
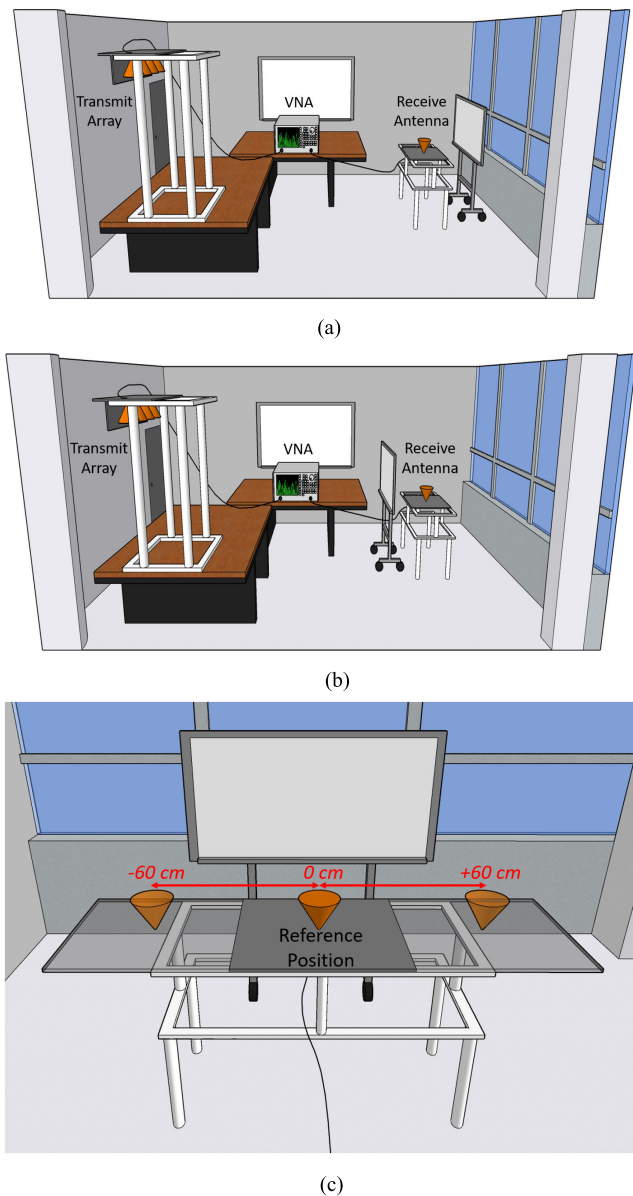
(a)

(b)

(c)

**FIGURE 6.** An illustrated view of the meeting room used for the propagation experiment with the measurement setup: (a) Line-of-sight (LOS) scenario. (b) Non-line-of-sight (NLOS) scenario. (c) Lateral range in which the receive antenna position is varied during the experiment.

## III. EXPERIMENT SETUP

The experiment consists of two stages, namely a) the wave propagation stage performed in an actual indoor environment where the signal transmission between the transmit array and receive antenna are measured, and b) the rectification stage where the corresponding received signals are fed into a rectifier to measure DC voltage and power conversion efficiency.

### A. WAVE PROPAGATION STAGE

The wave propagation stage is carried out in an office meeting room (7.35 m ×3.2 m ×2.5 m) furnished with scattering objects such as desks, columns and white boards as shown in Fig. 6. One of the four walls in the room is mostly composed of glass windows. The transmit array of four monoconical

elements and receive antenna (also a monocone) are placed towards two diagonally opposite corners of the room. Here, we use a monoconical antenna for its simplicity in design and fabrication, but a miniaturized antenna (e.g. flat antennas) should be more suitable in practical scenarios. However, the choice of antenna design is not a major factor in determining the performance of BF vs. TR, and our experimental results should qualitatively apply to any antenna types without loss of generality. Two representative scenarios, i.e. line-of-sight (LOS) and non-line-of-sight (NLOS), are considered as shown in Fig. 6(a) and Fig. 6(b) respectively. Between LOS and NLOS, the respective locations of the transmit array and receive antenna remains unchanged, while a portable white board is placed between the antennas to obstruct the direct path for the NLOS configuration. In each scenario, the position of the receive antenna is linearly scanned to observe the spatial variation of received power. Based on the free space wavelength $\lambda_0$ of 30 cm at the center frequency $f_0$ of 1 GHz (the center operating frequency in the experiment), the receive antenna position is varied at an increment of $0.2\lambda_0$ (6 cm) from the reference position (0 cm) to $\pm 2\lambda_0 (\pm 60$ cm) as shown in Fig. 6(c). The reference position of the receive antenna is 3.5 m in down range and 1.5 m in cross range from the center of the transmit array.

Figs. 7(a) and 7(b) respectively show the monoconical antenna used as the receive antenna and its reflection coefficient, which exhibits good impedance characteristics over 0.5 – 1.5 GHz. The monoconical antenna has an omnidirectional pattern in azimuth and a 3 dB beamwidth of 65° in elevation. The transmit array is constructed using four of this monoconical antenna is shown in Fig. 7(c). The array spacing is $\lambda_0/2(15$ cm), and a vertical ground plane is added to minimize backward radiation.

The propagation measurement is carried out one transmit-receive antenna pair at a time, which are combined through processing. To ensure the highest quality of the channel impulse responses for the analysis purpose, the measurement is done in the frequency domain using an Agilent 8720ES vector network analyzer. That is, the transfer function between each transmit element and receive antenna pair $S_{r,n}(\omega)$ is measured over a bandwidth of 0.5 – 1.5 GHz, which is then converted into the time-domain impulse response $h_n(t)$. The received signals for BF and TR, i.e. $y_{BF}(t)$ and $y_{TR}(t)$ are obtained in the processing using the respective equations presented in the previous section. Such a processing should mimic the case of actual signal transmission through BF and TR. It is assumed that a narrowband (CW) signal with $f_0$ is used for BF, and a Gaussian short pulse with a bandwidth of 500 MHz centered at $f_0$ is used for TR. In addition, for a reasonable comparison of BF and TR in the following rectification stage, the source average power at the transmitter is set to 30 dBm (1 Watt) for both cases.

### B. RECTIFICATION STAGE

In the rectification stage, the resulting time-domain signals $y_{BF}(t)$ and $y_{TR}(t)$ from the propagation stage are used as
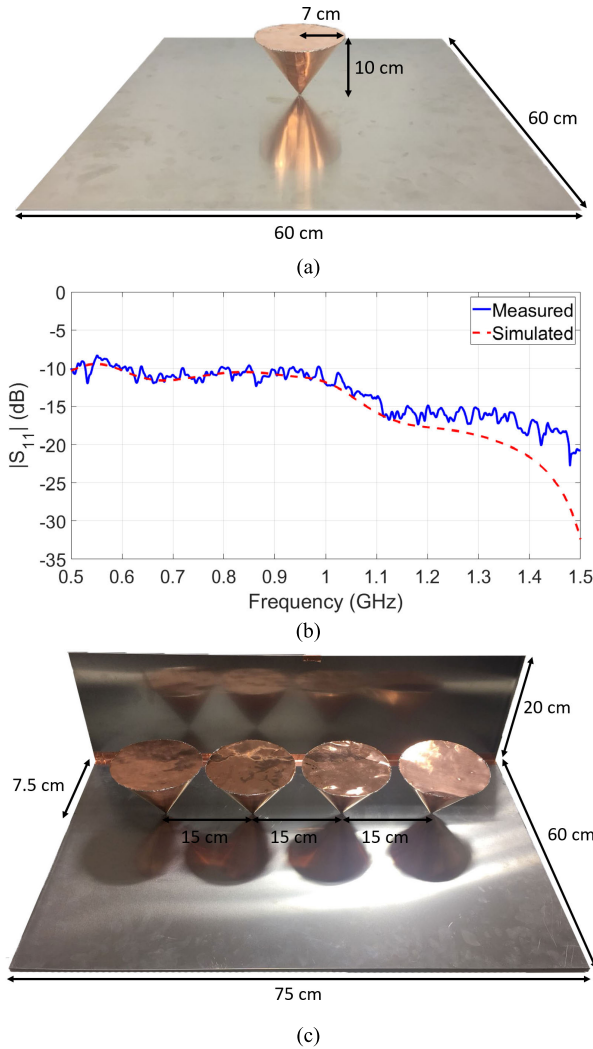
(a)



(b)



(c)

**FIGURE 7.** (a) Fabricated monoconical antenna used as the receive antenna, (b) reflection coefficient ($|S_{11}|$) of the monoconical antenna, and (c) fabricated 4-element array (of the same monoconical elements) used as the transmit antenna.



(a)



(b)

**FIGURE 8.** (a) Rectification measurement setup showing a picture of the broadband RF-to-DC rectifier used in the measurement, and (b) the reflection coefficient ($|S_{11}|$) of the rectifier.

input signals to an RF-to-DC rectifier, and the rectification efficiency between BF and TR is compared. The rectifier used in this experiment is specifically designed to cover a broad bandwidth [30], which allows for rectification of both narrowband signals and wideband pulses from BF and TR, respectively. The experiment setup consists of an arbitrary waveform generator (Tektronix AWG7102) as the waveform source followed by an amplifier (Mini-Circuits ZX60-123LN-S+) feeding the wideband rectifier whose output is connected to a voltmeter (Mastech MS8261) to measure rectified DC voltage, as shown in Fig. 8(a). The broadband rectifier is a voltage doubler based circuit with a series inductor connected to each diode to achieve broadband matching. Fig. 8(b) shows $|S_{11}|$ of the rectifier, which exhibits an impedance bandwidth of 76 % (from 0.61 to 1.36 GHz). The wide bandwidth of the rectifier allows for rectification of both
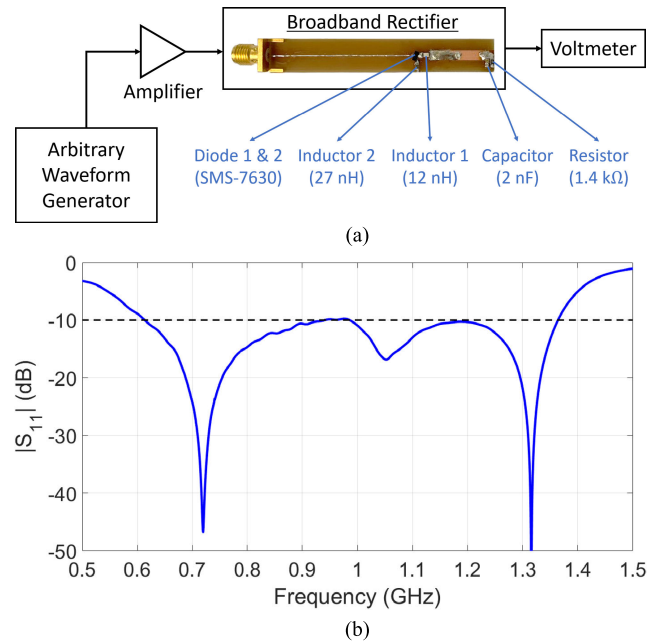
narrowband signals from BF and wideband pulses from TR. More detail on the design of the rectifier can be found in [30].

The signal level from AWG is set to reflect 30 dBm of average power at the transmitter for both BF and TR. The average power of the RF input at the rectifier for each case is

$$P_{in,BF} = \frac{1}{2} \frac{(\max |y_{BF}(t)|)^2}{Z_{in}}$$

$$P_{in,TR} = \frac{1}{T} \int_0^T \frac{y_{TR}^2(t)}{Z_{in}} dt, \qquad (17)$$

where $\max |y_{BF}(t)|$ is the peak voltage amplitude of $y_{BF}(t)$, $T$ is the TR pulse interval (length of recorded $b_n(t)$) which is set to 50 ns, and $Z_{in}$ is the input impedance set to 50 Ω. The rectification efficiency can then be calculated as

$$\eta_{BF} = \frac{P_{DC,BF}}{P_{in,BF}} = \frac{V_{DC,BF}^2}{R_L} \frac{1}{P_{in,BF}}$$

$$\eta_{TR} = \frac{P_{DC,TR}}{P_{in,TR}} = \frac{V_{DC,TR}^2}{R_L} \frac{1}{P_{in,TR}} \qquad (18)$$

where $P_{DC,BF}$ and $P_{DC,TR}$ are the DC power delivered to the load, $V_{DC,BF}$ and $V_{DC,TR}$ are the DC voltage at the load, and $R_L$ is the load resistance of 1.4 kΩ (optimal value for this rectifier [30]).

## IV. WAVE PROPAGATION RESULTS
### A. NUMERICAL SIMULATION
Prior to the measurement, BF and TR are examined via numerical simulation in an effort to gain a qualitative insight into the field behavior in wave propagation. The simulation is carried out with SEMCAD X [31], a finite difference time
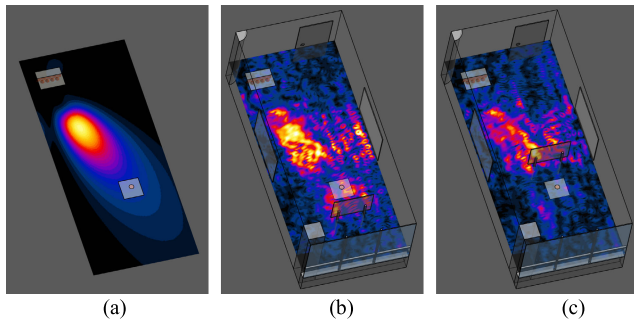
**FIGURE 9.** Simulated steady-state electric field intensity from BF for the receive antenna as shown in the figure: (a) Free space, (b) LOS in the room and (c) NLOS in the room.



**FIGURE 10.** Magnitude of the simulated electric fields from BF as a function of lateral position for five different targeted receive locations: (a) LOS scenario and (b) NLOS scenario.

domain full-wave simulation platform. A 3D model of a room with objects and walls that approximately represents the actual meeting room used for the measurement is constructed and simulated. Note that the simulated model does not exactly correspond to the experimental room down to every detail, since the purpose here is to provide a qualitative analysis of wave propagation in a complex environment and there is no merit in exactly modeling the actual room. For both BF and TR, the amplitudes of the transmit signals $x_{n,BF}(t)$ and $x_{n,TR}(t)$ are set to correspond to the average source power of 30 dBm.

In the case of BF, the values of $\phi_n$ are assumed to correctly represent (1), neglecting any phase distortion in the reception of a beacon signal, which allows us to focus on the wave propagation and beam impairment only during power transmission. Fig. 9 shows the simulated steady-state electric field intensity as a result of BF in three different scenarios, namely a) free space, b) LOS and c) NLOS. Here, the targeted receive antenna location is at the center position in Fig. 6(c). The free space scenario (without the room and scattering objects) provides a reference case in which the intended beam is generated perfectly towards the direction of the receive antenna, as shown in Fig. 9(a).

On the other hand, for both the LOS and NLOS scenarios in the room, the simulated electric field intensity as respectively shown in Figs. 9(b) and 9(c) indicates that the intended beam is impaired due to multipath, despite the use of $\phi_n$ that correctly represent the direction of the receive antenna. The fields are rather distributed over a wider area with a modal behavior (peaks and nulls). The field distribution in this case is directly related to the eigenmodes of the room that are determined by the size and boundary conditions. For LOS, the fields seem to slightly maintain the shape of a beam, but they never properly reach the receiver.

Now, the BF simulation is performed as the targeted receive location is varied linearly in the range of $\pm 2\lambda$ ($\pm 60$ cm) as in Fig. 6(c). For each targeted receive location, the transmit array is phased with the values of $\phi_n$ associated with the corresponding $\theta$. In Fig. 10, the resulting electric field magnitude as a function of lateral position is plotted for five different targeted receive locations for the LOS and NLOS scenarios.
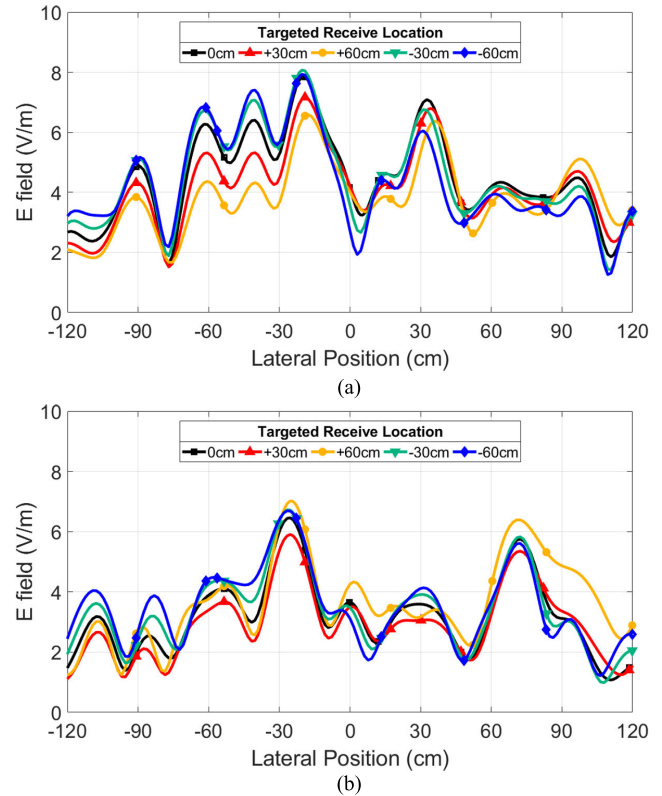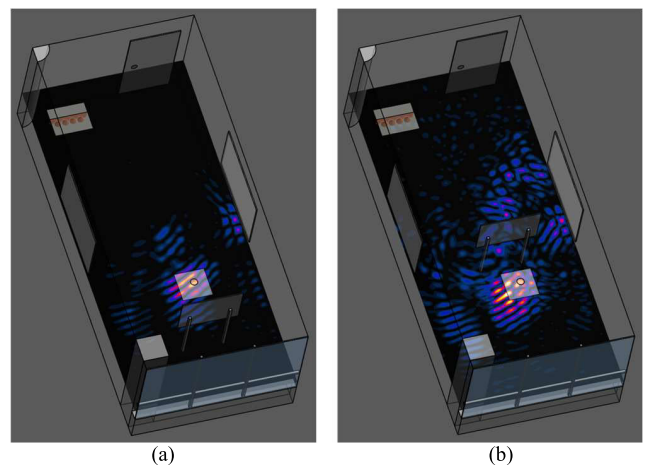


**FIGURE 11.** Simulated electric field intensity from TR for the receive antenna as shown in the figure at a time instance where wave focusing takes place: (a) LOS in the room and (b) NLOS in the room.

Despite the use of different values of $\phi_n$ in the transmit array for all five receive locations, the field distribution remains nearly identical for both LOS and NLOS. Such a phenomenon is attributed to the eigenmodes that are determined only by the geometry and boundary conditions in the room, regardless of how the fields are injected into the room. This clearly shows the impact of multipath on beamforming to a point where the beam is impaired and selective transmission to a particular location is made difficult.
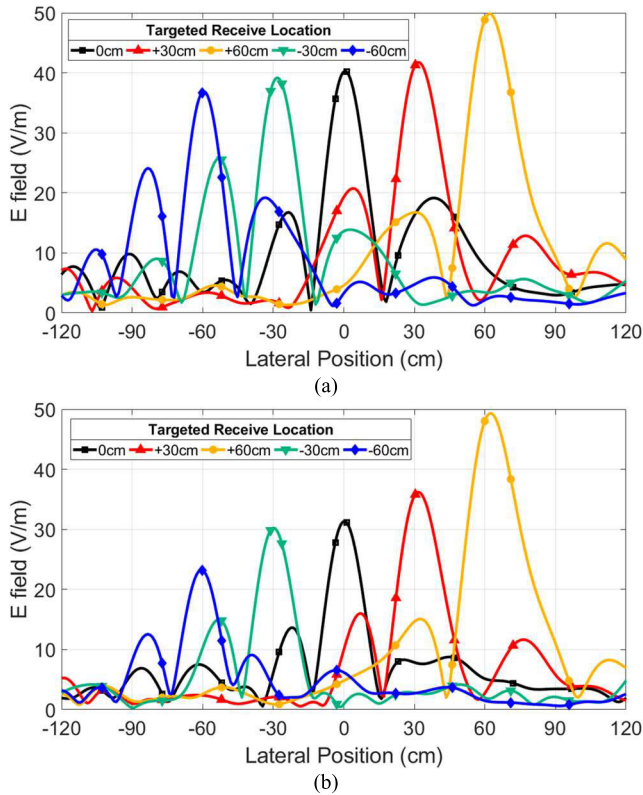
**FIGURE 12.** Magnitude of the simulated electric fields from TR as a function of lateral position for five different targeted receive locations: (a) LOS scenario and (b) NLOS scenario.

For TR, the transmit signals as defined in (7) are used, which are basically the time-reversed impulse responses between the transmit elements and receive antenna. Fig. 11 shows the simulated electric field intensity resulting from TR at a time instance where the waves focus at the location of the receive antenna for a) LOS and b) NLOS. Note that this wave focusing is due to the transmission from a single array element, as TR operates in a switched mode. The targeted receive antenna position is the same as that considered in Fig. 9 for BF. There is no point in considering free space for TR as it is used take advantage of multipath. Also, note that the field intensity plots are shown at a time instance instead of the steady state magnitude since wave focusing occurs in both space and time. In both scenarios, wave focusing does take place at the location of the receive antenna. That is, the field intensity is localized at the receiver while considerably low at other locations, indicating a successful selective transmission of electromagnetic power to the receive antenna.

The TR simulation is also performed as the targeted receive location is varied laterally in the range of $\pm 2\lambda$ ($\pm 60$ cm) in the same way as in BF. For each targeted receive location, the transmit array radiates a different set of $x_{n,TR}(t)$ associated with the location. In Fig. 12, the resulting electric field magnitude as a function of lateral position is plotted for five different targeted receive location for LOS and

NLOS. In contrast to BF, a peak consistently appears at the desired receive location for all five cases, indicating that TR enables wave focusing regardless of the receive location and LOS/NLOS conditions in a complex propagation environment.

### B. MEASUREMENT

As mentioned previously, the measurement is carried out in the frequency domain using a vector network analyzer by obtaining the transfer function $S_{r,n}(\omega)$, and both BF and TR are carried out in the processing to ensure the highest quality of signals for analysis. Accordingly, the phasing of the array elements for BF and generation of time-reversed signals for TR are done through signal processing without additional experimental devices. In an actual WPT scenario, BF requires a phase shifter for phasing the array elements and TR requires an arbitrary waveform generator to generate time-reversed waveforms.

The signal amplitudes of $x_{n,BF}(t)$ and $x_{n,TR}(t)$ are also set to represent the average source power of 30 dBm. Here, the targeted receive locations are scanned laterally as shown in Fig. 6(c) similar to the simulation, but at 11 different locations over the range of $\pm \lambda$ ($\pm 30$ cm) at an increment of $0.2\lambda$ (6 cm).

In Fig. 13, the peak values of the receive signals $y_{BF}(t)$ and $y_{TR}(t)$ (for both LOS and NLOS) as a function of lateral position are plotted for all 11 cases of targeted receive locations. Qualitatively, the measured results are in good agreement with the simulated results showing a similar trend. That is, the spatial pattern resulting from BF remains almost identical in all 11 cases for both LOS and NLOS, validating that the wave behavior in this multipath environment is dominated by the eigenmodes, thereby impairing the beam. The modal behavior of the fields is clearly observable with relative peaks and nulls taking place. For the spatial pattern resulting from TR, a distinct peak consistently occurs at the desired receive location for all 11 cases for both LOS and NLOS, validating the ability of TR for selective focusing of waves at desired locations. Fig. 14 shows *PRPR* calculated at each targeted receive location for both LOS and NLOS using (10). For both LOS and NLOS, the values of *PRPR* generally stay significantly greater than 1, indicating that TR delivers higher peak power compared to BF. Also, the *PRPR* values are higher for NLOS, due to a larger proportion in the received peak power between TR and BF. This implies that the advantage of TR over BF is further enhanced in NLOS conditions.

In terms of the relative peak voltage levels in both scenarios (LOS and NLOS), TR delivers higher peak voltage at the desired receive location compared to BF for all 11 cases given the same average transmit power. Moreover, TR selectively delivers peak power at the intended receiver location (selective focusing) regardless of its location, while BF does not show much of selectivity due to impairment of the beam. These results demonstrate that TR can not only perform better in a single transmit antenna case [17], [20], [26], but can also outperform array-based beamforming in selectively
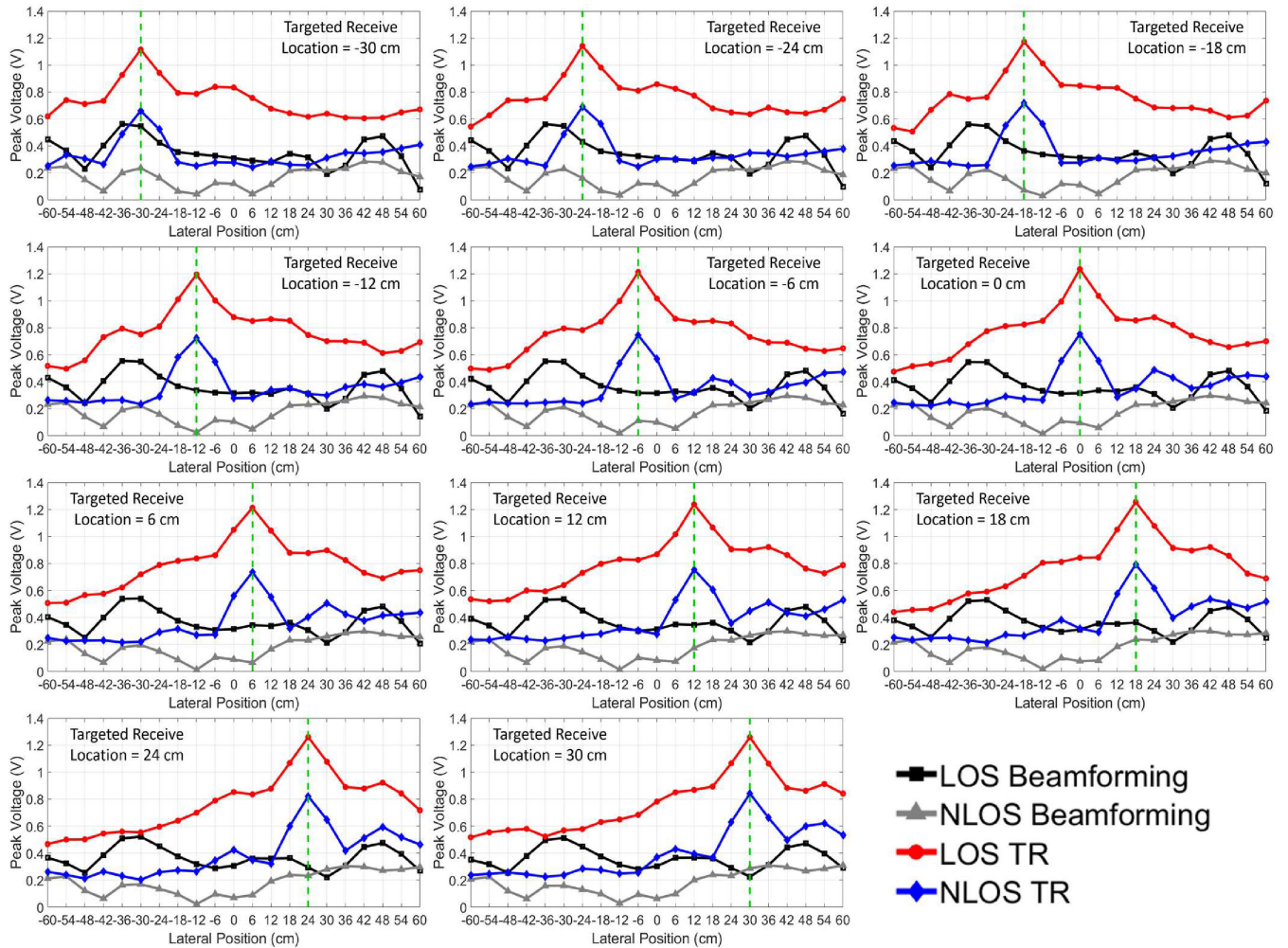
**FIGURE 13.** Measured peak voltage at the receiver as a function of lateral position resulting from BF and TR (for both LOS and NLOS).
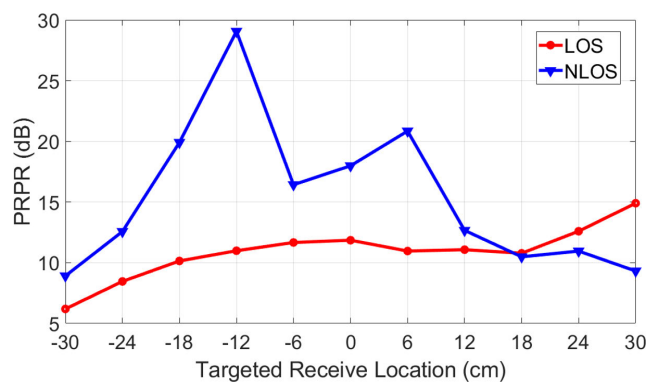


**FIGURE 14.** PRPR obtained from measured peak voltages at each targeted receive antenna location for both LOS and NLOS.



**FIGURE 15.** Measured DC voltage at each targeted receive antenna location for BF and TR (for both LOS and NLOS).

delivering higher peak power in a complex propagation environment.

## V. RECTIFICATION RESULTS

Using the experiment setup shown in Fig. 8(a), the received signals from the propagation stage, i.e. $y_{BF}(t)$ and $y_{TR}(t)$, are

taken as the input signals for the rectifier, and the rectified DC voltage $V_{DC,BF}$ and $V_{DC,TR}$ are measured. The resulting DC power and rectification efficiency are obtained using (17) and (18). Fig. 15 shows the DC voltage measured at the load versus the targeted receive locations for BF and
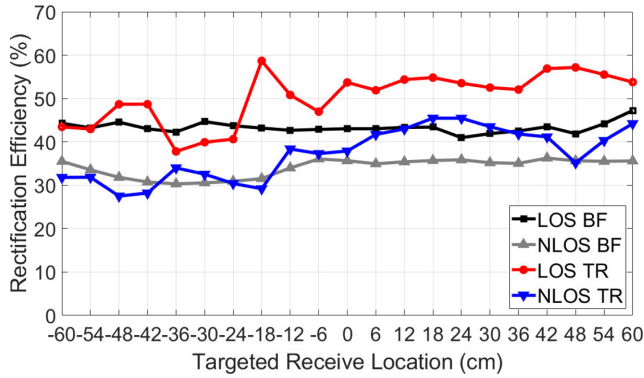
**FIGURE 16.** Measured rectification efficiency at each targeted receive antenna location for BF and TR (for both LOS and NLOS).



**FIGURE 17.** (a) Normalized impulse responses and (b) normalized magnitude of the transfer functions for strong, medium and weak multipath cases.

TR. In both the LOS and NLOS scenarios, TR produces higher rectified DC voltage than BF, that is, $y_{TR}(t)$ contains higher peak voltage compared to $y_{BF}(t)$ as a result of wave focusing. Since rectification is based on the voltage across the diode exceeding the junction potential of the diode, higher peak voltage leads to more rectification, producing higher DC voltage at the load. Therefore, it can be concluded that given the same average transmit power, TR delivers higher peak voltage as a result of wave focusing that allows for more effective rectification of RF to DC compared to BF in a complex propagation environment. The value of $V_{DC,TR}$ for NLOS increases as the receive position moves to the right, while other values remain relatively constant as shown in Fig. 15. This is possibly due to the partial removal of obstruction (of direct path) as the receive antenna position shifts towards right, where the direct paths from some of the transmit elements are restored. This partial LOS condition results in higher received peak voltage and therefore higher DC voltage.

The rectification efficiency (i.e. $\eta_{BF}$ and $\eta_{TR}$) versus the receive locations is also plotted for LOS and NLOS as shown in Fig. 16. For both propagation scenarios, TR generally provides higher rectification efficiency compared to BF. However, there is some variation in the values of $\eta_{TR}$ depending on the receive location while $\eta_{BF}$ remains relatively constant. This can be explained by the fact that $y_{TR}(t)$ does vary with the receive position. It is not only the peak level of the pulses in $y_{TR}(t)$, but also the 'time sidelobes' (low-amplitude noise outside the reconstructed pulse) as indicated in Fig. 5. Higher time-sidelobe levels may result in higher $P_{in,TR}$, thereby decreasing the rectification efficiency.

The results from this experiment provides a general insight into the performance of TR vs. BF in WPT from an antenna array in a complex propagation environment. That is, TR allows for selective concentration of peak power at a desired receive location by taking advantage of multipath, while BF loses its ability to do so from impaired beams due to multipath. As a result, TR outperforms BF in delivering power at the load with higher rectification efficiency. By optimizing the TR pulse interval $T$, array configuration, and
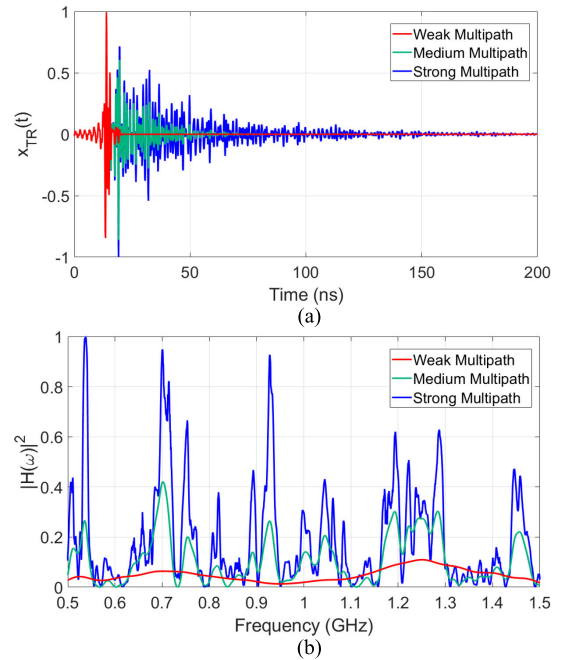
transmit power, the performance of TR-WPT may further be enhanced.

## VI. CONCLUSION
In this paper, we investigated the performance of time-reversal (TR) based wireless power transfer (WPT) from an antenna array in comparison to conventional beamforming (BF) based WPT in a complex propagation environment. Through the propagation experiment conducted in an indoor multipath environment, it was shown that TR allows for higher peak voltage at the receiver compared to BF given the same average transmit power. Furthermore, TR is shown to selectively deliver peak power at the intended receiver location, while BF does not show much of selectivity in power delivery due to the impaired beam. The results from the rectification stage of the experiment using a broadband rectifier show that the signals received using TR generally lead to higher rectified DC voltage and efficiency. The overall results imply that TR can outperform BF in selectively delivering power at the load with higher rectification efficiency. Further optimization of the TR pulse interval, array configuration, and transmit power may enhance the performance of TR based WPT in a complex propagation environment.

## APPENDIX
In this Appendix, we provide a qualitative analysis on *PRPR* to gain an insight into how it can be used as a performance metric for TR vs. BF. Here, we use one of the measured transfer functions and vary its signal decay factor to represent three different degrees of complexity in the propagation

**TABLE 1.** PRPR calculated for each multipath case.

| Multipath | PRPR | PRPR (dB) |
|-----------|------|-----------|
| **Weak** | 0.916 | -0.38 |
| **Medium** | 7.96 | 9.01 |
| **Strong** | 24.04 | 13.81 |

environment, i.e. strong, medium and weak multipath. Using (16), *PRPR* is calculated for these threes representative cases. The array element number $N$ is set to 4 as used in the experiment and $T$ is varied for each case depending on the decay level.

We use the impulse response $h(t)$ measured at the receive location of 12 cm (from the reference point) for NLOS. For the strong multipath case, $h(t)$ as measured is used. For the medium and weak multipath cases, the signal decay rate is altered by multiplying an exponential decay function $e^{-\alpha(t-t_0)}$, where different $\alpha$ values are used for the two respective cases. Here, $t_0$ corresponds to where the peak of the first received pulse occurs in $h(t)$.

Figs. 17(a) and 17(b) show the normalized impulse responses and magnitude of the transfer functions, respectively for the three representative cases. In Fig. 17(a), there is a clear difference in terms of signal length between the strong, medium and weak multipath cases. The signal slowly decays due to the reflected waves for strong multipath, while a set of only a few short pulses is present for weak multipath. In the transfer function plot in Fig. 17(b), multiple high-amplitude, closely-spaced modal peaks appear for strong multipath, while a low-level, relatively flat amplitude is seen across the bandwidth for weak multipath, as expected.

From these transfer functions, *PRPR* can be calculated for each multipath case using (16) and their values are shown in Table 1. These *PRPR* results are directly associated with the signal characteristics in Figs. 17(a) and 17(b). For strong and medium multipath, higher modal peaks in the transfer function and longer $T$ produce *PRPR* significantly greater than 1. However, for weak multipath, lower transfer function magnitudes and shorter $T$ due to the rapidly decaying impulse response result in *PRPR* less than (or near) 1. These results qualitatively validate (16) that the level of *PRPR* primarily depends on the complexity of the propagation environment.

In this regard, *PRPR* would be a great performance predictor for TR vs. BF WPT in a given environment, where one only needs the transfer function between the transmit array and receive antenna. The higher the value of *PRPR* the more likely it is for TR to outperform BF, and vice versa.

## REFERENCES

[1] W. C. Brown, "The history of power transmission by radio waves," *IEEE Trans. Microw. Theory Techn.*, vol. MTT-32, no. 9, pp. 1230–1242, Sep. 1984.

[2] Z. Popovic, "Cut the cord: Low-power far-field wireless powering," *IEEE Microw. Mag.*, vol. 14, no. 2, pp. 55–62, Mar. 2013.

[3] J. Garnica, R. A. Chinga, and J. Lin, "Wireless power transmission: From far field to near field," *Proc. IEEE*, vol. 101, no. 6, pp. 1321–1331, Jun. 2013.

[4] Z. Popovic, E. A. Falkenstein, D. Costinett, and R. Zane, "Low-power far-field wireless powering for wireless sensors," *Proc. IEEE*, vol. 101, no. 6, pp. 1397–1409, Jun. 2013.

[5] X. Lu, D. Niyato, P. Wang, and D. I. Kim, "Wireless charger networking for mobile devices: Fundamentals, standards, and applications," *IEEE Wireless Commun.*, vol. 22, no. 2, pp. 126–135, Apr. 2015.

[6] H. Dinis, I. Colmiais, and P. Mendes, "Extending the limits of wireless power transfer to miniaturized implantable electronic devices," *Micromachines*, vol. 8, no. 12, p. 359, 2017.

[7] D. Belo, D. C. Ribeiro, P. Pinho, and N. B. Carvalho, "A selective, tracking, and power adaptive far-field wireless power transfer system," *IEEE Trans. Microw. Theory Techn.*, vol. 67, no. 9, pp. 3856–3866, Sep. 2019.

[8] H. Zhai, H. K. Pan, and M. Lu, "A practical wireless charging system based on ultra-wideband retro-reflective beamforming," in *Proc. IEEE Antennas Propag. Soc. Int. Symp.*, Toronto, ON, Canada, Jul. 2010, pp. 1–4.

[9] X. Wang, S. Sha, J. He, L. Guo, and M. Lu, "Wireless power delivery to low-power mobile devices based on retro-reflective beamforming," *IEEE Antennas Wireless Propag. Lett.*, vol. 13, pp. 919–922, May 2014.

[10] J. He, X. Wang, L. Guo, S. Shen, and M. Lu, "A distributed retro-reflective beamformer for wireless power transmission," *Microw. Opt. Technol. Lett.*, vol. 57, no. 8, pp. 1873–1876, Aug. 2015.

[11] X. Wang, B. Ruan, and M. Lu, "Retro-directive beamforming versus retro-reflective beamforming with applications in wireless power transmission," *Prog. Electromagn. Res.*, vol. 157, pp. 79–91, Jan. 2016.

[12] Y. Li and V. Jandhyala, "Design of retrodirective antenna arrays for short-range wireless power transmission," *IEEE Trans. Antennas Propag.*, vol. 60, no. 1, pp. 206–211, Jan. 2012.

[13] K. Xu, Z. Shen, Y. Wang, X. Xia, and D. Zhang, "Hybrid time-switching and power splitting SWIPT for full-duplex massive MIMO systems: A beam-domain approach," *IEEE Trans. Veh. Technol.*, vol. 67, no. 8, pp. 7257–7274, Aug. 2018.

[14] K. Xu, Z. Shen, M. Zhang, Y. Wang, X. Xia, W. Xie, and D. Zhang, "Beam-domain SWIPT for mMIMO system with nonlinear energy harvesting legitimate terminals and a non-cooperative terminal," *IEEE Trans. Green Commun. Netw.*, vol. 3, no. 3, pp. 703–720, Sep. 2019.

[15] S. Ding, S. Gupta, R. Zang, L. Zou, B.-Z. Wang, and C. Caloz, "Enhancement of time-reversal subwavelength wireless transmission using pulse shaping," *IEEE Trans. Antennas Propag.*, vol. 63, no. 9, pp. 4169–4174, Sep. 2015.

[16] F. Cangialosi, T. Grover, P. Healey, T. Furman, A. Simon, and S. M. Anlage, "Time reversed electromagnetic wave propagation as a novel method of wireless power transfer," in *Proc. IEEE Wireless Power Transf. Conf. (WPTC)*, Aveiro, Portugal, May 2016, pp. 1–4.

[17] R. Ibrahim, D. Voyer, A. Breard, J. Huillery, C. Vollaire, B. Allard, and Y. Zaatar, "Experiments of time-reversed pulse waves for wireless power transmission in an indoor environment," *IEEE Trans. Microw. Theory Techn.*, vol. 64, no. 7, pp. 2159–2170, Jul. 2016.

[18] Z.-W. Lin, B.-J. Hu, Z.-H. Wei, and P. Liao, "An optimal time reversal waveform based on sequential convex programming for wireless power transmission," in *Proc. IEEE 18th Int. Conf. Commun. Technol. (ICCT)*, Chongqing, China, Oct. 2018, pp. 916–920.

[19] H. S. Park, H. Y. Hong, and S. K. Hong, "Smart far-field wireless power transfer via time reversal," *J. Korean Inst. Electromagn. Eng. Sci.*, vol. 29, no. 4, pp. 285–289, Apr. 2018.

[20] S. K. Hong, V. M. Mendez, T. Koch, W. S. Wall, and S. M. Anlage, "Nonlinear electromagnetic time reversal in an open semireverberant system," *Phys. Rev. A, Gen. Phys.*, vol. 2, no. 4, Oct. 2014, Art. no. 044013.

[21] M. Fink, "Time reversal of ultrasonic fields. I. Basic principles," *IEEE Trans. Ultrason., Ferroelectr., Freq. Control*, vol. 39, no. 5, pp. 555–566, Sep. 1992.

[22] F. Wu, J.-L. Thomas, and M. Fink, "Time reversal of ultrasonic fields. II. Experimental results," *IEEE Trans. Ultrason., Ferroelectr., Freq. Control*, vol. 39, no. 5, pp. 567–578, Sep. 1992.

[23] G. Lerosey, J. de Rosny, A. Tourin, A. Derode, G. Montaldo, and M. Fink, "Time reversal of electromagnetic waves," *Phys. Rev. Lett.*, vol. 92, no. 19, May 2004, Art. no. 193904.

[24] G. Lerosey, J. de Rosny, A. Tourin, A. Derode, and M. Fink, "Time reversal of wideband microwaves," *Appl. Phys. Lett.*, vol. 88, no. 15, Apr. 2006, Art. no. 154101.

[25] A. Khaleghi, "Measurement and analysis of ultra-wideband time reversal for indoor propagation channels," *Wireless Pers. Commun.*, vol. 54, no. 2, pp. 307–320, Jul. 2010.

[26] M.-L. Ku, Y. Han, H.-Q. Lai, Y. Chen, and K. J. R. Liu, "Power waveforming: Wireless power transfer beyond time reversal," *IEEE Trans. Signal Process.*, vol. 64, no. 22, pp. 5819–5834, Nov. 2016.

[27] E. Falkenstein, M. Roberg, and Z. Popovic, "Low-power wireless power delivery," *IEEE Trans. Microw. Theory Techn.*, vol. 60, no. 7, pp. 2277–2286, Jul. 2012.

[28] A. Boaventura, D. Belo, R. Fernandes, A. Collado, A. Georgiadis, and N. B. Carvalho, "Boosting the efficiency: Unconventional waveform design for efficient wireless power transfer," *IEEE Microw. Mag.*, vol. 16, no. 3, pp. 87–96, Apr. 2015.

[29] R. Ibrahim, D. Voyer, M. El Zoghbi, J. Huillery, A. Breard, C. Vollaire, B. Allard, and Y. Zaatar, "Novel design for a Rectenna to collect pulse waves at 2.4 GHz," *IEEE Trans. Microw. Theory Techn.*, vol. 66, no. 1, pp. 357–365, Jan. 2018.

[30] H. S. Park and S. K. Hong, "Broadband RF-to-DC rectifier with uncomplicated matching network," *IEEE Microw. Wireless Compon. Lett.*, vol. 30, no. 1, pp. 43–46, Jan. 2020.

[31] X. Semcad. *EM Simulation Platform*. Accessed: Jan. 15, 2020. [Online]. Available: https://speag.swiss/products/semcad/overview/

**HONG SOO PARK** (Student Member, IEEE) received the B.S. degree (Hons.) in electronic engineering from Soongsil University, Seoul, South Korea, in 2019, where he is currently pursuing the degree in electronic engineering under the combined M.S./Ph.D. Program. His research interests include wireless power transfer, antennas, microwave and millimeter-wave devices, electromagnetic time-reversal, and electromagnetics in complex environment.

Mr. Park received four poster awards with the Korean Institute of Electromagnetic Engineering and Sciences (KIEES) conferences, in 2017, 2018, and 2019.

**SUN K. HONG** (Member, IEEE) received the B.S. degree in electrical engineering from the University of Maryland, College Park, MD, USA, in 2005, and the M.S. and Ph.D. degrees in electrical engineering from Virginia Tech, Blacksburg, VA, USA, in 2008 and 2012, respectively.

From 2005 to 2015, he was a Research Engineer with the U.S. Naval Research Laboratory, Tactical Electronic Warfare Division, Washington, DC, USA, where he has been started as an undergraduate Research Intern and assumed a Leading Role, since 2008, in various research projects related to time-domain techniques in electromagnetics, nonlinear electromagnetic interaction, radars, electromagnetic scattering, high-power microwave (HPM) applications, and antennas. From 2015 to 2017, he was an Assistant Professor with the Department of Electrical and Computer Engineering, Rose-Hulman Institute of Technology, Terre Haute, IN, USA. He was appointed as an Assistant Professor with Soongsil University, Seoul, South Korea, in 2017, where he is currently an Assistant Professor with the School of Electronic Engineering. His current research interests include wireless power transfer, electromagnetic waves in complex propagation environment, detection of nonlinear devices, radars and high-power electromagnetics, and antennas. He has authored/coauthored more than 20 research articles in refereed journals and a number of conference papers presented with the international conferences.

Dr. Hong received the Alan Berman Research Publication Award, in 2014 and 2015, and the NRL Invention Award, in 2015. He also received a Letter Appreciation from the Commanding Officer of NRL, for his contribution to Counter-IED Technology, in 2013.

• • •